HHS Public Access

Author manuscript

Nat Commun. Author manuscript; available in PMC 2015 January 28.

Published in final edited form as:

Nat Commun. ; 5: 4487. doi:10.1038/ncomms5487.

Receptor interacting protein 140 attenuates endoplasmic reticulum stress in neurons and protects against cell death

Xudong Feng[1], **Kelly A. Krogh**[1], **Cheng-Ying Wu**[1], **Yi-Wei Lin**[1], **Hong-Chieh Tsai**[1,2], **Stanley A. Thayer**[1], and **Li-Na Wei**[1,*]

[1] Department of Pharmacology, University of Minnesota Medical School, Minneapolis, MN 55455, USA

[2] Department of Neurosurgery, Chang-Gung Memorial Hospital and University, Tao-Yuan, Taiwan, R.O.C

Abstract

Inositol 1, 4, 5-trisphosphate receptor (IP_3R)-mediated Ca^{2+} release from the endoplasmic reticulum (ER) triggers many physiological responses in neurons and when uncontrolled can cause ER stress that contributes to neurological disease. Here we show that the unfolded protein response (UPR) in neurons induces rapid translocation of nuclear receptor-interacting protein 140 (RIP140) to the cytoplasm. In the cytoplasm, RIP140 localizes to the ER by binding to the IP_3R. The carboxyl-terminal RD4 domain of RIP140 interacts with the carboxyl-terminal gate-keeping domain of the IP_3R. This molecular interaction disrupts the IP_3R's “head-tail” interaction, thereby suppressing channel opening and attenuating IP_3R-mediated Ca^{2+} release. This contributes to a rapid suppression of the ER stress response and provides protection from apoptosis in both hippocampal neurons *in vitro* and in an animal model of ER stress. Thus, RIP140 translocation to the cytoplasm is an early response to ER stress and provides protection against neuronal death.

Keywords

IP_3R; RIP140; ER stress; hippocampal neuron; calcium homeostasis

Introduction

Ca^{2+} release mediated by the inositol 1, 4, 5-trisphosphate receptor (IP_3R) is critical to cellular signal propagation[1]. However, uncontrolled Ca^{2+} release from the endoplasmic reticulum (ER) triggered by IP_3R dysfunction or ER stress elevates intracellular Ca^{2+}

* Correspondence Dr. Li-Na Wei, Department of Pharmacology, 6-120 Jackson Hall, 321 Church St. SE, Minneapolis, MN 55455, USA Tel: 612-6259402 Fax: 612-6258408 weixx009@umn.edu.

Contributions

L.-N Wei and X.-D Feng designed the study; X.-D Feng, K.A. Krogh, C.-Y. Wu, Y.-W Lin and H.-C. Tsai performed experiments; X.-D Feng and K.A. Krogh collected and analyzed data; X.-D Feng, wrote the manuscript; L.-N Wei and S.A. Thayer provided reagents, technical support, and conceptual advice.

Competing financial interests

The authors declare no competing financial interests.

concentration ($[Ca^{2+}]_i$) resulting in toxicity and cell death[2]. Thus, regulation of IP_3R activity is vital to Ca^{2+} homeostasis and cell survival. Disruption of ER Ca^{2+} homeostasis contributes to cell death in the progression of neurological disease[3, 4]. Depletion of ER Ca^{2+} stores results in ER stress that evokes the unfolded protein response (UPR). Deregulation of the UPR elevates expression of CCAAT/enhancer binding protein homologous protein (CHOP) resulting in ER-dependent apoptosis[5]. Conversely, blockade of ER Ca^{2+} release by dantrolene and xestospongin C, inhibitors of ryanodine receptor (RyRs) and IP_3Rs respectively, prevents prion and amyloid-beta(Aβ)-induced neuronal death[6, 7]. Furthermore, inhibition of IP_3R-mediated Ca^{2+} release attenuates ER stress and improves cell survival following SERCA inhibition[8].

In mammals, there are three IP_3R subtypes: IP_3R1, 2, and 3. IP_3R1 is the predominant subtype expressed in the cerebellum and hippocampus[9, 10]. IP_3R activity is regulated by proteins residing in the ER lumen or the cytosol[11]. Similar to other Ca^{2+} channels, the functional IP_3R exists as a tetramer. Its primary structure is divided into three domains: the NH2-terminal ligand-binding domain (LBD), the coupling domain, and the carboxyl-terminal channel gate domain (CGD). ER Ca^{2+} release through the IP_3R channel is regulated by the actions of accessory modulating proteins that can interact with the large cytosolic regions of the LBD and the CGD under both normal and certain pathologic conditions[12, 13]. The positive modulating proteins include neuronal calcium sensor 1 (NCS1), huntington, and cytochrome *c*, which enhance channel opening and Ca^{2+} release[14, 15]. In contrast, the IP_3R-binding protein released with IP_3 (IRBIT) is a pseudo-ligand that suppresses the activity of IP_3Rs by competing with IP_3 binding[16]. Moreover, the anti-apoptotic protein Bcl-2 inhibits IP_3-dependent channel opening and Ca^{2+} release by interacting with the CGD and the coupling domain of the IP_3R[17]. Blocking Ca^{2+} transfer from the ER to mitochondria by IP_3R-binding proteins, GIT1 and GIT2, attenuates cell death[18]. However, how IP_3R is negatively regulated, which can be neuroprotective, following channel over-activation remains unclear.

Receptor-interacting protein 140 (RIP140), a wide-spectrum transcription co-regulator, is highly expressed in multiple tissues including the brain[19]. Its primary physiological action is to negatively regulate hormonal control of gene activity by recruiting repressive chromatin remodeling machinery in the presence of hormones, thereby triggering hormone-elicited gene suppression[20, 21]. Interestingly, the expression of RIP140 decreases with aging[22]. RIP140 knockout mice exhibit learning and memory deficits and increased stress responses[23]. Additionally, elevated RIP140 levels in the hippocampi of patients with Down syndrome [24] suggest physiological or pathological relevance of RIP140 in the brain. But the action of RIP140 in neurons remains unclear. In dissecting the molecular mechanisms underlying RIP140's functions, we have systemically examined this protein in various cellular contexts and found that it is extensively modified by post-translational modifications (PTMs) in a context-dependent manner. These include various forms of phosphorylation[25], lysine and arginine methylation[26], lysine-vitamin B conjugation[27], lysine acetylation and sumoylation[28, 29], and ubiquitination[30]. Most of these PTMs modulate RIP140's regulation of gene expression/chromatin remodeling in the nucleus, which is consistent with its principal activity as a transcriptional co-regulator. However, a novel signaling pathway

rapidly stimulates the export of RIP140 from the nucleus to the cytoplasm where it then becomes a cytosolic regulator. This pathway is triggered by specific serine phosphorylation on Ser^{102} and Ser^{1003} followed by arginine methylation on Arg^{240}, Arg^{650} and Arg^{948} [30]. In adipocytes, cytosolic RIP140 can interact with AS160, an Akt substrate, to suppress glucose transporter 4 (GLUT4) and adiponectin vesicle trafficking, thereby reducing glucose uptake and adiponectin secretion[31].

Considering the high levels of neuronal RIP140 expression, the behavioral phenotypes of RIP140 knockout mice, and the gradual decline of RIP140 in aging brain, we hypothesized that RIP140 is important for the proper function of neurons. In this study, we observed rapid stress-induced export of RIP140 from the nucleus to the cytosol in neurons. The cytosolic RIP140 is an early, neuroprotective IP_3R-interacting protein. By binding to IP_3R to suppress its channel opening, cytosolic RIP140 helps to attenuate IP_3R-mediated Ca^{2+} release. We also demonstrate the physiological relevance of this mechanism in ER stress models *in vitro* and *in vivo*.

Results

ER stress triggers RIP140 nuclear export and localization to the ER

RIP140 is exported from the nucleus to the cytoplasm of adipocytes following sequential PTMs initiated by PKCε-dependent phosphorylation[32]. We found that in neurons, the UPR triggered the translocation of RIP140 to the cytoplasm. We applied several *in vitro* ER stress inducers to hippocampal neurons. Thapsigargin (Tg) depletes ER Ca^{2+} by blocking ER membrane Ca^{2+} pumps; dithiothreitol (DTT) is a reducing agent; brefeldin A (BFA) induces ER stress by collapse of the Golgi into the ER; and tunicamycin (Tm) inhibits N-linked glycosylation. Treating mouse hippocampal neural cells (HT22 cells) with Tg, DTT, or BFA increased cytoplasmic RIP140 levels while simultaneously decreasing nuclear RIP140 levels (Fig.1 a-c). Aβ neurotoxicity involves elevated ER stress[33]. Interestingly, RIP140 translocation can also be triggered by aggregated Aβ peptide ($Aβ_{1-40}$ and $Aβ_{1-42}$) in hippocampal neurons. As shown in Fig. 1d, using Lentivirus carrying GFP-RIP140, we detected GFP-RIP140 mainly in the nucleus, which was translocated to the cytoplasm following Aβ treatment for 24 h. To rule out the potential translational effect on the elevation of RIP140 in the cytoplasm, we applied a translational inhibitor cycloheximide (CHX). Fig. 1e and f shows that pretreatment of cells with CHX did not block the increase of RIP140 in the cytoplasm. Since nuclear export of RIP140 could be triggered by PKCε-initiated phosphorylation of RIP140, we examined the effects of Tg on RIP140 (CN), a mutant previously shown defective in nuclear export in adipocytes[34]. We also employed a PKC inhibitor to examine whether this PKC pathway was involved in nuclear export of RIP140 in the stressed neurons. Fig. 1g confirms that the nuclear export-deficient mutant RIP140 failed to translocate out of the nucleus in Tg-treated cells. Fig. 1h further supports this notion because the PKC inhibitor (CHE) blocked nuclear export of RIP140 in Tg-treated cells. These experiments demonstrate that in stressed hippocampal neurons, RIP140 is exported from the nucleus to the cytoplasm via a PKC-mediated nuclear export pathway.

Next, to study the distribution of cytoplasmic RIP140, we measured the endogenous RIP140 levels in different sub-cellular fractions derived from HT22 cells following UPR induced by

Tg, DTT, and Tm. These data all show that both endogenous RIP140 (detected by western blot using anti-RIP140 antibody) and exogenous RIP140 (transfected by Lentivirus and detected by GFP fluorescence) target ER following ER stress (Fig. 2).

Cytoplasmic RIP140 interacts with the IP_3R

Since the elevated cytosolic RIP140 increasingly accumulated on ER following UPR, we then determined the cytoplasmic protein that might bind RIP140 by performing a yeast two-hybrid screen. Using RIP140 as the bait we identified IP_3R as a RIP140-interacting protein. We then examined the nature of RIP140 interaction with IP_3R by monitoring its localization to the ER. Fig. 3a shows that RIP140 was detected in the ER fraction but was no longer detectable in the proteinase K-treated ER fraction, in contrast to the intra-membrane protein, calnexin, and the ER lumen protein, Bip, which remained intact following proteinase K treatment. Thus, RIP140 localizes to the outer-membrane of the ER. We then determined the interacting domains of RIP140 and IP_3R in HT22 cells. Fig. 3b shows the constructs of RIP140 and IP_3R used in these reciprocal protein interaction assays. The results of coimmunoprecipitation (co-IP) assays show that RIP140 could be detected only when lysate was co-precipitated with the C-terminal gate-keeping domain of IP_3R (CT), indicating that CT is the target of RIP140 binding (Fig. 3c). A series of truncated mutants of RIP140 were examined for their interaction with IP_3R-CT in HT22 cells. As show in Fig.3d, RIP140 mutant lacking RD4 (RD1-3) failed to interact with IP_3R-CT, suggesting that RD4 of RIP140 is essential and sufficient for its binding to IP_3R-CT. This finding was further confirmed by *in vitro* direct protein interaction assays (Supplementary Fig. 1). We then hypothesized that the interaction between RIP140 and IP_3R might be disrupted by the specific RD4 motif of RIP140. To test this hypothesis, we employed a competitive co-IP assay by over-expressing RD4 in HT22 cells and monitoring the formation of endogenous RIP140/IP_3R complex using an antibody specific for the N-terminus of RIP140 and the IP_3R antibody (Fig. 3e). In the presence of exogenously provided RD4 or RIP140 that contains RD4 (RD3-4), the formation of endogenous RIP140/IP_3R complex, as indicated by the reciprocally precipitated RIP140 or IP_3R, was inhibited. Since RD4 of RIP140 is essential and sufficient to mediate the interaction of RIP140 with IP_3R, we next evaluated the potential function of RD4 motif in response to ER stress. Transfected flag-tagged full-length RIP140 (RD1-4) and RD4 were detected by immunofluorescence assay using flag antibody. As show in Supplementary Fig. 2, RD4 was initially homogenous distributed in nuclei and cytoplasm, and remained evenly distributed following ER stress. As predicted, full-length RIP140 was translocated to cytoplasm and interacted with IP_3R upon ER stress. These results show that RD4 can interact with IP_3R, but it lacks the signal for translocation in response to ER stress. Finally, we used an *in situ* proximity ligation assay (PLA) to examine the kinetics of endogenous IP_3R1-RIP140 complex formation during Tg-induced ER stress. This assay employed two antibodies, anti-RIP140 and anti-IP_3R, followed by the addition of specific oligonucleotides that could be amplified into fluorescent signals[35]. Only when the two antibodies existed in close proximity (<40 nm) could amplification be successful as indicated by fluorescent signals[36]. Thus, the appearance of fluorescent signal indicates the formation and location of the molecular complex containing specific components recognized by IP_3R and RIP140 antibodies. As shown in Fig. 3f, Tg rapidly induced the formation of endogenous RIP140/IP_3R1 complex, which was attenuated by pretreating cells with the

PKC inhibitor, CHE. The co-IP in Fig. 3g shows the time-dependent formation of RIP140/IP_3R1 complex following Tg-treatment, in agreement with the time-dependent association described in the PLA assay. These results show that stress promotes RIP140 export from the nucleus to the cytoplasm where it localizes to the ER and binds the gate-keeping domain of IP_3R via RIP140's RD4 domain.

RIP140 attenuates ER Ca^{2+} release in neurons

Because RIP140 translocated to the ER in response to stress and interacted with the IP_3R, we suspected that RIP140 might regulate IP_3R function. To examine this possibility, primary hippocampal neurons were transfected with plasmids encoding DsRed2 plus RIP140 (n=7 coverslips, 8 cells) or DsRed2 only (n=4 coverslips, 4 cells) as an expression control. Non-expressing neurons (n=11 coverslips, 686 cells) in the same imaging field served as a control (Fig. 4 A-E). Twenty-four hours after transfection, neurons were loaded with fura-2 and then $[Ca^{2+}]_i$ was recorded using digital imaging. Basal $[Ca^{2+}]_i$ remained stable in non-expressing neurons and in neurons expressing RIP140 or DsRed2 at 79 ± 3 nM, 68 ± 12 nM, and 40 ± 4 nM, respectively. After recording stable basal $[Ca^{2+}]_i$ for 1 minute, Ca^{2+} influx via voltage-gated Ca^{2+} channels was evoked by applying a 15 s depolarizing stimulus (50 mM K^+). The depolarization-induced increase in $[Ca^{2+}]_i$ was 722 ± 123 nM, 858 ± 366 nM, and 606 ± 182 nM for non-expressing neurons, neurons expressing RIP140, or DsRed2, respectively. This transient increase in the $[Ca^{2+}]_i$ showed that RIP140 expression did not affect voltage-gated Ca^{2+} channel function or $[Ca^{2+}]_i$ clearance mechanisms and also served to uniformly load ER Ca^{2+} stores[37]. After returning to basal $[Ca^{2+}]_i$, the group I metabotropic glutamate receptor (mGluR) agonist DHPG (30 μM) was superfused for 30 s. Activation of group I mGluRs activates phospholipase C to generate IP_3 and mobilize ER Ca^{2+} in hippocampal neurons[38]. As shown in figure 4, DHPG evoked a rapid increase in $[Ca^{2+}]_i$ that quickly returned to basal $[Ca^{2+}]_i$ in the maintained presence of the agonist. A secondary response was observed in some cells, which is consistent with IP_3-evoked $[Ca^{2+}]_i$ oscillations described for these cells[39]. Expression of RIP140 attenuated DHPG-evoked Ca^{2+} release relative to non-expressing neurons or neurons expressing DsRed2. To confirm that DHPG was evoking Ca^{2+} release via activation of the IP_3R, we applied DHPG in the presence of the IP_3R antagonist, xestospongin C (10 μM). DHPG-evoked Ca^{2+} release was blocked by xestospongin C (n=5 coverslips, 168 cells) relative to untreated control (n=3 coverslips, 155 cells; data not shown). We next examined the role of RIP140 in regulating the release of Ca^{2+} from ER stores in the HT22 cell line that was used for the preceding translocation and biochemical studies. Thapsigargin (Tg)-evoked Ca^{2+} release was recorded from HT22 cells expressing RIP140 (n=3 coverslips, 114 cells) or a RIP140 mutant (RIP140 RD4-neg) (n=4 coverslips, 169 cells) that lacks the IP_3R-binding domain (Fig. 4 F-G). Non-expressing cells (n=12 coverslips, 779 cells) served as a control. Basal $[Ca^{2+}]_i$ remained stable in non-expressing cells and cells expressing RIP140 or RIP140(RD4-neg) at 85 ± 2 nM, 101 ± 2 nM, and 109 ± 5 nM, respectively. After recording stable basal $[Ca^{2+}]_i$ for 5 minutes, ER Ca^{2+} release was evoked by applying Tg (1 μM). Tg evoked a transient increase in $[Ca^{2+}]_i$ that returned to basal levels in the maintained presence of the drug. Expression of RIP140 attenuated Tg-evoked Ca^{2+} release relative to non-expressing cells or cells expressing RIP140 (RD4-neg). Taken together, these data indicate

that RIP140 attenuates ER Ca^{2+} release in hippocampal neurons and in HT22 cells via an IP_3R-dependent mechanism and in a manner dependent on its RD4 domain, respectively.

Cytoplasmic RIP140 suppresses the "head-tail" interaction of IP_3R

It is well established that binding of IP_3 to the IP_3R promotes a "head-tail" interaction in which the cytoplasmic amino- and carboxyl- termini interact, resulting in channel opening[40]. Since RIP140 bound to the C-terminal gate-keeper domain of IP_3R and inhibited IP_3-induced Ca^{2+} release without altering IP_3 binding to IP_3R (Supplementary Fig. 3), we hypothesized that RIP140 might inhibit the "head-tail" interaction of the IP_3R. We first tested this notion using recombinant proteins in *in vitro* competition assays, and asked if RD4 domain could prevent IP_3R-NT from binding to IP_3R-CT. As shown in Fig.5 a, immunoprecipitation of HA-tagged IP_3R-CT pulled down flag- tagged IP_3R-NT. Adding RD4 domain (in various concentrations, + and ++) increasingly abolished IP_3R-CT interaction with IP_3R-NT. On the contrary, adding the same amount of RIP140 RD1-3 domain failed to inhibit IP_3R-CT binding to IP_3R-NT. Thus, RD4 of RIP140 can inhibit IP_3R-CT binding to IP_3R-NT in a dose-dependent manner. Since RIP140 cytoplasmic translocation is the early response to ER stress, cytoplasmic localized RIP140 may act to disrupt IP_3R-CT and NT interaction. This was confirmed by co-IP assay in HT22 cells that, over-expressing mutant RIP140 (CN), which cannot translocate to cytoplasm, failed to inhibit IP_3R-CT and -NT interaction (Fig.5b). To examine the "head-tail" interaction of endogenous IP_3R, we overexpressed or silenced endogenous RIP140, and employed *in situ* PLA assay to follow the endogenous IP_3R's "head-tail" interaction using antibodies against the N-terminus and the C-terminal gate region of IP_3R. As shown in Fig. 5 c and d, in both control transfections (SiCtrl and Vector), m-3M3FBS (m-3M3), which increases IP_3 levels by activating phospholipase C (PLC), increased the number of fluorescent puncta indicative of positive "head-tail" interaction resulting from the activation of endogenous IP_3R. The increased fluorescent puncta were further enhanced following RIP140 knockdown (Fig.5c), but were blocked upon RIP140 overexpression (Fig.5d). These data show that RIP140 negatively regulates IP_3R-mediated channel opening by interfering with the "head-tail" interaction of IP_3R.

RIP140-IP_3R interaction protects neurons against ER stress

Considering that stress promotes translocation of RIP140 to the cytoplasm to interact with the IP_3R and that over-expressing RIP140 attenuates IP_3R-mediated Ca^{2+} release, we speculated that the cytoplasmic RIP140 might protect cells from ER stress. To examine this notion, we inhibited the interaction of RIP140 with IP_3R and then measured the ER stress response in HT22 cells. Several strategies were used to inhibit RIP140 interaction with IP_3R including: siRNA-mediated knockdown of RIP140 (SiRIP140), expressing a mutant RIP140 that is deficient in nuclear export (CN), or expressing a truncation mutant of RIP140 that lacks the RD4 domain (RD1-3). Fig. 6a shows that Tg induced ER stress in the control cell (SiCtrl) as indicated by up-regulated expression of Bip, ATF4, CHOP, and phosphorylated eIF2a. These stress-induced changes were enhanced by knockdown of RIP140 (SiRIP140). In consistence with this observation, treatment of cultured hippocampal neurons with aggregated Aβ peptide increased the expression of CHOP, and the level of CHOP was further elevated in RIP140 deficit neurons (Supplementary Fig. 4). These results indicate

that RIP140 plays a protecting role against Aβ neurotoxicity. To validate the neuroprotective effect of RIP140 against stress-induced apoptosis, we monitored cell apoptosis by pSIVA-PI double staining. pSIVA detects cell surface phosphatidylserine, an early marker for apoptosis and propridium iodide (PI) labels the nuclei of dead cells. Fig. 6b and c show that knockdown of RIP40 increased ER stress resulting in an increased number of cells labeled for pSIVA and PI. Importantly, Fig. 6d shows that expressing the mutant RIP140 (CN and RD4 deleted RIP140) increased the extent of ER stress relative to expressing wild-type RIP140 (RIP140-WT), as indicated by the elevation of ER stress markers phosphorylated eIF2α (p-eIF2α) and CHOP. Furthermore, compared to wild-type RIP140, mutant RIP140 (RIP140-CN) failed to protect cells from ER stress-induced apoptosis (Fig. 6 e, f). These results demonstrate that RIP140 protects cells from ER stress.

Loss of RIP140 enhances ER stress-induced neuronal death

To validate the functional role for RIP140 in protecting neurons from ER stress *in vivo*, we employed an animal model of ER stress induced by intraperitoneal injection of Tg[41]. Lentivirus carrying shRNA against RIP140 was injected stereotaxically to knockdown endogenous RIP140 in the CA1 region of the hippocampus as depicted in Fig. 7a. Fig. 7b (top) and Supplementary Fig. 5 confirmed the reduction in RIP140 protein level in animals injected with shRNA against RIP140 (shRIP140). ER stress was elicited 3 or 18 days after Lentivirus delivery of shRNA, and analyses of the hippocampus were conducted 2 days later. Fig. 7b (panels 2-6) show elevated ER stress related proteins, including Bip, phosphorylated eIF2a (p-eIF2a), ATF4, and CHOP in Tg-treated control (without silencing RIP140) animals. The RIP140-silenced animals (shRIP140, 5 days post Lentivirus injection), even without Tg induction, exhibited elevated ER stress markers that were enhanced by treatment with Tg. Cells from RIP140 knockdown mice (20 days post Lentivirus injection) exhibited increased apoptosis upon Tg treatment (Fig. 7c and d). These animal studies validate a functional role for RIP140 in neuroprotection against ER stress *in vivo*.

Discussion

RIP140 is highly expressed in metabolic tissues and the brain. The physiological role for RIP140 in metabolism is primarily mediated by its nuclear receptor coregulator activity that regulates insulin sensitivity and inflammatory responses in adipocytes and macrophages[31]. How RIP140 may function in the brain has not been determined. This study reveals rapid nuclear export of RIP140 to the cytoplasm in ER-stressed hippocampal neurons. The study also reports a new functional role for cytoplasmic RIP140 in neurons. RIP140 attenuates ER stress by interacting with IP_3R through the carboxyl terminal RD4 domain of RIP140 and the C-terminal gate-keeping domain of the IP_3R. This interaction interferes with IP_3R's "head-tail" interaction, thereby suppressing Ca^{2+} release and preventing neuronal death. Finally, the physiological relevance of this novel protective mechanism against Aβ neurotoxicity and ER stress was demonstrated in hippocampal neuron cultures and an animal model.

Our previous studies showed a specific signaling pathway regulating the phosphorylation of RIP140, which triggers nuclear export of RIP140 in adipocytes[26]. The signaling pathway is initiated by activated nuclear PKCε, which specifically phosphorylates Ser^{102} and Ser^{1003} of RIP140, followed by arginine methylation on Arg^{240}, Arg^{650} and Arg^{948} [34]. PKCε is broadly expressed in neuronal tissue and is regarded as a stress sensor[42, 43]. Increased cytosolic Ca^{2+} causes PKCε activation, which plays protective roles against hypoxia and excitatory neurotoxicity[44]. Interestingly, activation of PKCε protects neurons from ER stress-induced apoptosis[45]. In the present study, hippocampal neurons appear to engage the PKCε–dependent pathway to stimulate RIP140's nuclear export upon ER stress. Both inhibiting PKCε and mutating RIP140 to abrogate its PKC-elicited nuclear export can abolish the protective function of RIP140 in stressed neurons. Of significance is the observation that acute ER-stress readily triggers nuclear export of RIP140 in hippocampal neurons, which can be a new signaling pathway mediating PKCε action as a stress sensor to protect neurons from ER stress-induced cell death. This may represent a fundamental, stress-elicited physiological mechanism to rapidly resolve acute ER stress in neurons. However, it remains to be determined whether this may provide any protection during chronic ER stress. The fate of the exported RIP140 following its binding to the IP_3R also awaits further study.

With respect to the molecular mechanism, it is known that IP_3R activity is controlled by the direct association of its head and tail in both homo- and hetero-tetrameric complexes[12, 40, 46]. Interestingly, this can be regulated by RIP140 via a direct interaction with the IP_3R C-terminal gate-keeper domain, which disrupts the “head-tail” interaction and then suppresses channel opening and Ca^{2+} release. Importantly, a simple RD4 epitope is sufficient to reduce the formation of endogenous RIP140/IP_3R complex. Thus, the RIP140 RD4 domain interaction with the C-terminal gate-keeper domain of the IP_3R may serve as a potential therapeutic target in diseases related to ER stress. ER homeostasis is regulated by Ca^{2+} uptake and efflux through various transporters and ion channels on the ER membrane that are modulated by intracellular signaling cascades[47, 48]. Depleting the ER Ca^{2+} store by blocking ER membrane Ca^{2+} pumps or through uncontrolled ER Ca^{2+} release results in ER stress and cell death, which is believed to contribute to the development of neurodegenerative disease[49, 50]. Activating IP_3Rs is known to trigger pathological processes, including apoptosis[51]. A recent study showed that loss of IP_3R1 enhances neuronal vulnerability to ER stress via a mitochondria-dependent pathway in an animal model[52]. Furthermore, stimulation of ER Ca^{2+} release channels accelerates Tg-induced ER depletion and apoptosis[53] and reducing Ca^{2+} release from ER by pharmacologically blocking IP_3R-mediated Ca^{2+} release following treatment with a SERCA inhibitor attenuated ER stress and improved cell survival[8]. These studies demonstrate complicated regulation of IP_3R in normal and stressed conditions. Despite an in-depth understanding of IP_3R activation by its binding partner[54], much less is known about the negative regulation of the IP_3R. The present study describes a new physiological pathway, initiated by ER stress, in which nuclear export of RIP140 provides an immediate negative regulatory mechanism to attenuate IP_3R activity and the subsequent stress response. While RIP140 does not seem to affect IP_3 binding to IP_3R (Supplemental Figure 3), it remains to be determined whether and how RIP140 may affect the action of other IP_3R-regulatory molecules implicated in the regulation of IP_3R-mediated Ca^{2+} release, such as cytochrome *c* and bcl-2[55, 56].

IP_3R-mediated Ca^{2+} release is regulated by IP_3R modulatory proteins that can act on either cytosolic or luminal sites[17, 57]. Intralumenal proteins, such as ERp44 and chromogranin, are typically involved in long-term chronic stress[58]. Ca^{2+}-dependent apoptosis is regulated by ER oxidase 1-a (ERO1-a) that disrupts the interaction between ERp44 and IP_3R in prolonged ER stress[59]. Interaction of the IP_3R with cytosolic proteins, like cytochrome c and bcl-2, represents a delayed response following ER stress[17, 60]. RIP140 is a different type of cytosolic regulator of the IP_3R because it acts by rapidly attenuating the IP_3R "head-tail" interaction immediately following stress induction. How this newly identified mechanism may be integrated with other IP_3R-modulatory events in order to maintain the homeostasis of IP_3R activity remains to be determined.

Materials and methods

Cell cultures

Primary hippocampal neurons were isolated as previously described[61]. Briefly, the hippocampal tissues from embryonic (E16-18) mice brain were dissociated with 0.25% trypsin and cultured on poly-d-lysine coated plates in neurobasal medium supplemented with B27. The experiments were carried after 12-14 days of culture (DIV 12-14). HT22 cells (from Salk Institute) were maintained with DMEM supplemented with 10% FBS and differentiated in neurobasal medium with N2 supplement for 3 days before treatment.

$[Ca^{2+}]_i$ imaging

Intracellular Ca^{2+} concentration ($[Ca^{2+}]_i$) was recorded as previously described[62] with minor modifications. Cells (DIV12-14) were loaded with fura-2 by incubation in hepes-buffered Hanks' salt solution (HHSS) containing 5 μM fura-2 acetoxymethyl ester in 0.04% pluronic acid for 30 min at 37 °C followed by washing in the absence of indicator for 10 min. Coverslips containing fura-2 loaded cells were transferred to a recording chamber, placed on the stage of an Olympus IX71 microscope (Melville, NY), and viewed through a 20X objective. Excitation wavelength was selected with a galvanometer-driven monochromator (8-nm slit width) coupled to a 75-W xenon arc lamp (Optoscan; Cairn Research). $[Ca^{2+}]_i$ was monitored using sequential excitation of fura-2 at 340 and 380 nm; image pairs were collected every 1 s. For experimental recordings, cells were superfused at a rate of 1-2 mL/min with HHSS for 2 min followed by a 15 s perfusion of 50 mM K^+ to depolarize the neurons and equally load the endoplasmic reticulum (ER) with Ca^{2+}. Ca^{2+} release from IP_3-sensitive stores was evoked by 30 s superfusion with 30 μM DHPG. Ca^{2+} release from the ER of HT22 cells was evoked by Tg diluted in HHSS and bath applied to a final concentration of 1 μM. Fluorescence images (510/40 nm) were projected onto a cooled charge-coupled device camera (Cascade 512B; Roper Scientific) controlled by MetaFluor software (Molecular Devices). After background subtraction, the 340- and 380-nm image pairs were converted to $[Ca^{2+}]_i$ using the formula $[Ca^{2+}]_i = K_d\beta(R-R_{min})/(R_{max}-R)$ where R is 340 nm/380 nm fluorescence intensity ratio. The dissociation constant used for fura-2 was 145 nM, and β was the ratio of fluorescence intensity acquired with 380 nm excitation measured in the absence and presence of Ca^{2+}. R_{min}, R_{max}, and β were determined in a series of calibration experiments on intact cells by applying 10 μM ionomycin in Ca^{2+}-free buffer (1 mM EGTA) and saturating Ca^{2+} (5 mM Ca^{2+}). Values for R_{min}, R_{max}, and β were

0.37, 9.38, and 6.46, respectively. These calibration constants were applied to all experimental recordings. The neuronal cell body was selected as the region of interest for all recordings. All neurons within imaging fields were included in the analysis and no exclusions were made. To generate pseudocolor images, a binary mask was generated by applying an intensity threshold to the 380 nm image and applied to $[Ca^{2+}]_i$ images with colors assigned as indicated by the calibration bars in the figures.

Plasmids and siRNAs

Flag- or HA-tagged full length and truncated constructs of RIP140 corresponding to different lengths (see Fig.3 b) were generated by PCR from mouse cDNA and subcloned into the site of BamHI and NheI of pCMX-PL1 (System Biosciences). The primers for RIP140 are: 5'-GGCAGCAAACCTGAATTCGGC-3' (sense), 5'-CTCACCGGGCACG GAACATC-3' (antisense). cDNA encoding the N-terminal coupling domain(IP_3R1/NT, aa 1-225) and C-terminal gate keeping domain of IP_3R1 (IP_3R1/CT, aa 2590–2749) were generated by PCR from mouse cDNA and subcloned into the site of EcoR1 and Kpn1 of pCMX-PL1. Constitutive nuclear export negative mutation of RIP140 (CN) involving residues Ser-102 and Ser-1003 was made using QuikChange XL site-directed mutagenesis kit (Stratagene). The mutagenic primers are: S102A: 5'-CGGAAGAGGCT GGCTGATGCCATCGTG-3' (sense), 5'-CACGATGGCATCAGC CAGCCTCTTCCG-3' (antisense); S1003A: 5'-CATAGGACATTTGCATACCCGGG AATG-3' (sense), 5'-CATTCCCGGGTATGCAAATGTCCTATG-3' (antisense). Scrambled RNA and siRNAs for Nrip1 (5'- CGGCGTTGACATCAAAGAA-3' and 5'-GCTTCTTTCTTTAATCTAA-3', SI02698759) were from Qiagen.

Lentivirus production, concentration and transduction

Full length RIP140 or shRIP140 (target sequence: 5'-CCCGGCGTTGACATCAAAGAA-3' and 5'-AAGCTTCTTTCTTTAA-3') was subcloned into the site of NotI and XbaI of pCDH-GFP (System Biosciences) to generate RIP140 overexpression or RIP140 silence lentiviral vectors. Lentivirus was concentrated and titled as described[63]. Briefly, 293T cells were transfected with expression vectors (full length RIP140 or shRIP140) and packaging vectors (System Biosciences). Lentivirus-containing medium was collected at 24, 48 and 72 h after transfection. Viral particles were concentrated by ultracentrifugation and purified through a sucrose cushion (20% sucrose in HBSS). Concentrated and purified virus was suspended in HBSS and stored at −80°C. For transduction, neurons were incubated with lentivirus for 16 h and then the medium was replaced with fresh culture medium.

Cell transfection

Mouse primary hippocampal neurons were transfected between 12-14 days *in vitro* using a modification of a calcium phosphate protocol. Briefly, hippocampal cultures were incubated for 30 min in DMEM supplemented with 1 mM kynurenic acid, 10 mM $MgCl_2$, and 5 mM HEPES. A DNA/calcium phosphate precipitate containing 1 μg plasmid DNA per well was prepared, allowed to form for 30 min at 21°C then added to the culture. Following 90 min incubation, cells were washed once with DMEM supplemented with $MgCl_2$ and HEPES and then returned to conditioned media. HT22 cells were transfected with siRNA to knockdown

RIP140 using HiPeFect transfect reagent (301707, QIAGEN) according to the manufactural instruction. The plasmid DNA was transfected into HT22 cells using Lipofectamine® 2000 Transfection Reagent(11668019, Invitrogen) according to the manufacturer's instruction.

Western blotting

For western blotting, the cell lysates were prepared by sonication in RIPA buffer with protease and phosphatase inhibitor cocktails. Proteins (60-80 μg) were separated by 8 - 15% SDS-PAGE gel electrophoresis and transferred to PVDF membranes, blocked (in 5% milk) and incubated overnight in primary antibodies (information is provided in supplementary table 1) followed by respective anti-IgG secondary antibodies. Membranes were developed for visualization and photography using ECL reagent (Thermo). Optical band densities were quantified using Pro-Gel Image software and the result was analyzed using SPSS17.0 software. Uncropped images of all blots are shown in Supplementary Figures 5-14.

In situ proximal-ligation assay

In situ proximal-ligation assay was performed using Duolink PLA assay kit (Olink Bioscience) according to the protocol provided by the manufacturer. Briefly, cells were fixed using 4% poly-paraformaldehyde and incubated with primary antibodies overnight at 4°C. To detect the endogenous interaction of RIP140 with IP_3R1, anti-RIP140 (sc-8997; Santa Cruz; 1:200) and anti-IP_3R (sc-271197; Santa Cruz;1:200) were used. The IP_3R1 C- and N-terminal association was detected using antibodies recognize C-(407140, Calbiochem; 1:300) and N-terminus(LS-C121863, Lifespan; 1:300) of IP_3R1. Images were acquired by Olympus FluoView 1000 IX2 upright confocal microscope. The fluorescent punctae represents protein complex from different fields of individual experiment was counted with Image J image processing freeware (http://rsbweb.nih.gov/ij/), and the result was analyzed using SPSS17.0 software.

Subcellular Fractionation

Subcellular fractions including endoplasmic reticulum (ER), mitochondria and nuclear from cell or hippocampus were isolated using ER and mitochondria isolation kit (ER 0100 and MITOISO2, Sigma) according to the protocol.

Detection of apoptosis

Cell apoptosis was detected using CytoGLO™ SIVA-IANBD kit (IMG-6701K, IMGENEX) and CF™594 TUNEL apoptosis detection kit (30064, Biotium) according to the protocol. Images were acquired by Olympus FluoView 1000 IX2 upright confocal microscope. The fluorescence intensity representing pSIVA, PI and TUNEL-positive cell number from different fields was counted using Image J and quantified.

Aβ aggregation and cell treatment

The aggregation of peptide was described as previously[64]. Briefly, synthetic $Aβ_{1-40}$ and $Aβ_{1-42}$ (American Peptide, 62-0-86 and 62-0-80) were dissolved to 0.5 mg/mL in neurobasal medium and incubated for 4 d at 37°C. Cultured hippocampal neurons were incubated with 10 μM of aggregated peptide for 24 h and then immunofluorescence was performed.

In vitro competition assay

HA-tagged IP_3R-NT was synthesized *in vitro* using a coupled reticulocyte lysate system(TNT, promega) and incubated overnight at 4 C with the presence of flag-tagged IP_3R-CT. Sequential reactions were prepared with increasing amounts of flag-tagged RD4 synthesized in a TNT system present in reaction. Flag-tagged RD1-3 was added to the reaction as negative control. *In vitro* pull down assay was then performed and the protein levels of IP_3R-CT, RD4 and RD1-3 were determined by Western blot.

Animal experiments

Male adult C57BL/6 mice (8-9 weeks old), from Charles River Laboratories, were maintained and experimental procedures were conducted according to NIH guidelines and approved by the University of Minnesota Institutional Animal Care and Use Committee (Protocol no. 1007A86332). Lentivirus carrying RIP140-shRNA, was delivered to hippocampus using stereotaxic apparatus at anteroposterior (AP) 2.0 mm, medial-lateral (ML) 1.2 mm and dorsoventral (DV)1.6 mm according to previous describe[65]. RIP140 protein levels following virus injection were detected using immunofluorescence and western blot as indicated in the figure legend. The ER stress animal models were generated following intraperitoneal injection of Tg(1 μg/g) or normal saline(control) after 3 or 18 days of virus injection. Then the animals were anesthetized 2 days later and brain tissues were subjected to immunofluorescence staining or protein extraction. To detect the apoptotic cells, TUNEL staining of brain sections was performed using CF^{TM}594 TUNEL apoptosis detection kit (30064, Biotium). Images were acquired by Olympus FluoView 1000 IX2 upright confocal microscope. The TUNEL-positive cell numnber versus total cell number indicated by DAPI from the Lentivirus-infected areas was counted and quantified. Background was adjusted using Image J before counting.

Statistical Analyses

Statistical significance for multiple comparisons was determined by Student's *t*-test or ANOVA as indicated in the figure legend using SPSS17.0 software and summarized as the mean ± SEM of repeated measures, $p<0.05$ was considered statistically significant at the 95% level.

For $[Ca^{2+}]_i$ imaging studies, an individual experiment (n=1) was defined as the change in DHPG-evoked or Tg-evoked Ca^{2+} release from a single cell on a single coverslip. Changes in DHPG-evoked or Tg-evoked Ca^{2+} release are presented as mean ± SEM. Each experiment was replicated using at least 3 separate coverslips from at least 2 separate cultures. Significant differences were determined by one-way ANOVA with 3 levels followed by Tukey's *post hoc* test for multiple comparisons (OriginPro v8.5).

Supplementary Material

Refer to Web version on PubMed Central for supplementary material.

Acknowledgments

This work was supported by NIH grants DK54733 and DK60521, the Dean's commitment and Distinguished McKnight Professorship of University of Minnesota (L.- N. Wei) and by DA07304 (SAT). We thank technical assistance from X Chan, P.-C. Ho, Shawna Persaud, Y.-F. Kam and David Lin. A National Institute on Drug Abuse Training Grant (DA007097) supported KK.

References

1. Taylor CW, Tovey SC. IP3 Receptors: Toward Understanding Their Activation. Cold Spring Harbor perspectives in biology. 2010; 2:22.
2. Narayanan R, Dougherty KJ, Johnston D. Calcium store depletion induces persistent perisomatic increases in the functional density of h channels in hippocampal pyramidal neurons. Neuron. 2010; 68:921–935. [PubMed: 21145005]
3. Mekahli D, Bultynck G, Parys JB, De Smedt H, Missiaen L. Endoplasmic-Reticulum Calcium Depletion and Disease. Csh Perspect Biol. 2011; 3:1–32.
4. Bodalia A, Li H, Jackson MF. Loss of endoplasmic reticulum Ca2+ homeostasis: contribution to neuronal cell death during cerebral ischemia. Acta pharmacologica Sinica. 2013; 34:49–59. [PubMed: 23103622]
5. Tabas I, Ron D. Integrating the mechanisms of apoptosis induced by endoplasmic reticulum stress. Nature cell biology. 2011; 13:184–190. [PubMed: 21364565]
6. Ferreiro E, Resende R, Costa R, Oliveira CR, Pereira CM. An endoplasmic-reticulum-specific apoptotic pathway is involved in prion and amyloid-beta peptides neurotoxicity. Neurobiology of disease. 2006; 23:669–678. [PubMed: 16844381]
7. Ferreiro E, et al. Involvement of mitochondria in endoplasmic reticulum stress-induced apoptotic cell death pathway triggered by the prion peptide PrP(106-126). J Neurochem. 2008; 104:766–776. [PubMed: 17995926]
8. Dror V, et al. Glucose and endoplasmic reticulum calcium channels regulate HIF-1beta via presenilin in pancreatic beta-cells. The Journal of biological chemistry. 2008; 283:9909–9916. [PubMed: 18174159]
9. Cai W, et al. Activity-dependent expression of inositol 1,4,5-trisphosphate receptor type 1 in hippocampal neurons. The Journal of biological chemistry. 2004; 279:23691–23698. [PubMed: 15016804]
10. Mikoshiba K. IP3 receptor/Ca2+ channel: from discovery to new signaling concepts. J Neurochem. 2007; 102:1426–1446. [PubMed: 17697045]
11. Choe CU, Ehrlich BE. The inositol 1,4,5-trisphosphate receptor (IP3R) and its regulators: sometimes good and sometimes bad teamwork. Science's STKE : signal transduction knowledge environment. 2006; 2006:re15.
12. Uchida K, Miyauchi H, Furuichi T, Michikawa T, Mikoshiba K. Critical regions for activation gating of the inositol 1,4,5-trisphosphate receptor. The Journal of biological chemistry. 2003; 278:16551–16560. [PubMed: 12621039]
13. Schug ZT, Joseph SK. The role of the S4-S5 linker and C-terminal tail in inositol 1,4,5-trisphosphate receptor function. The Journal of biological chemistry. 2006; 281:24431–24440. [PubMed: 16815846]
14. Boehning D, et al. Cytochrome c binds to inositol (1,4,5) trisphosphate receptors, amplifying calcium-dependent apoptosis. Nature cell biology. 2003; 5:1051–1061. [PubMed: 14608362]
15. Schlecker C, et al. Neuronal calcium sensor-1 enhancement of InsP3 receptor activity is inhibited by therapeutic levels of lithium. The Journal of clinical investigation. 2006; 116:1668–1674. [PubMed: 16691292]
16. Ando H, et al. IRBIT suppresses IP3 receptor activity by competing with IP3 for the common binding site on the IP3 receptor. Molecular cell. 2006; 22:795–806. [PubMed: 16793548]
17. Rong YP, et al. The BH4 domain of Bcl-2 inhibits ER calcium release and apoptosis by binding the regulatory and coupling domain of the IP3 receptor. Proceedings of the National Academy of Sciences of the United States of America. 2009; 106:14397–14402. [PubMed: 19706527]

18. Zhang S, Hisatsune C, Matsu-Ura T, Mikoshiba K. G-protein-coupled receptor kinase-interacting proteins inhibit apoptosis by inositol 1,4,5-triphosphate receptor-mediated Ca2+ signal regulation. The Journal of biological chemistry. 2009; 284:29158–29169. [PubMed: 19706611]
19. Lee CH, Chinpaisal C, Wei LN. Cloning and characterization of mouse RIP140, a corepressor for nuclear orphan receptor TR2. Molecular and cellular biology. 1998; 18:6745–6755. [PubMed: 9774688]
20. Persaud SD, Huang WH, Park SW, Wei LN. Gene repressive activity of RIP140 through direct interaction with CDK8. Mol Endocrinol. 2011; 25:1689–1698. [PubMed: 21868449]
21. Park SW, Huang WH, Persaud SD, Wei LN. RIP140 in thyroid hormone-repression and chromatin remodeling of Crabp1 gene during adipocyte differentiation. Nucleic acids research. 2009; 37:7085–7094. [PubMed: 19778926]
22. Ghosh S, Thakur MK. Tissue-specific expression of receptor-interacting protein in aging mouse. Age (Dordr). 2008; 30:237–243. [PubMed: 19424847]
23. Duclot F, et al. Cognitive impairments in adult mice with constitutive inactivation of RIP140 gene expression. Genes, brain, and behavior. 2012; 11:69–78.
24. Gardiner K. Transcriptional dysregulation in Down syndrome: predictions for altered protein complex stoichiometries and post-translational modifications, and consequences for learning/behavior genes ELK, CREB, and the estrogen and glucocorticoid receptors. Behavior genetics. 2006; 36:439–453. [PubMed: 16502135]
25. Gupta P, Huq MD, Khan SA, Tsai NP, Wei LN. Regulation of co-repressive activity of and HDAC recruitment to RIP140 by site-specific phosphorylation. Molecular & cellular proteomics : MCP. 2005; 4:1776–1784. [PubMed: 16093479]
26. Mostaqul Huq MD, et al. Suppression of receptor interacting protein 140 repressive activity by protein arginine methylation. The EMBO journal. 2006; 25:5094–5104. [PubMed: 17053781]
27. Huq MD, Tsai NP, Lin YP, Higgins L, Wei LN. Vitamin B6 conjugation to nuclear corepressor RIP140 and its role in gene regulation. Nature chemical biology. 2007; 3:161–165. [PubMed: 17277785]
28. Rytinki MM, Palvimo JJ. SUMOylation modulates the transcription repressor function of RIP140. The Journal of biological chemistry. 2008; 283:11586–11595. [PubMed: 18211901]
29. Ho PC, et al. Modulation of lysine acetylation-stimulated repressive activity by Erk2-mediated phosphorylation of RIP140 in adipocyte differentiation. Cellular signalling. 2008; 20:1911–1919. [PubMed: 18655826]
30. Mostaqul Huq MD, Gupta P, Wei LN. Post-translational modifications of nuclear co-repressor RIP140: a therapeutic target for metabolic diseases. Current medicinal chemistry. 2008; 15:386–392. [PubMed: 18288993]
31. Ho PC, Lin YW, Tsui YC, Gupta P, Wei LN. A negative regulatory pathway of GLUT4 trafficking in adipocyte: new function of RIP140 in the cytoplasm via AS160. Cell metabolism. 2009; 10:516–523. [PubMed: 19945409]
32. Ho PC, Tsui YC, Lin YW, Persaud SD, Wei LN. Endothelin-1 promotes cytoplasmic accumulation of RIP140 through a ET(A)-PLCbeta-PKCepsilon pathway. Molecular and cellular endocrinology. 2012; 351:176–183. [PubMed: 22209746]
33. Nakagawa T, et al. Caspase-12 mediates endoplasmic-reticulum-specific apoptosis and cytotoxicity by amyloid-beta. Nature. 2000; 403:98–103. [PubMed: 10638761]
34. Gupta P, et al. PKCepsilon stimulated arginine methylation of RIP140 for its nuclear-cytoplasmic export in adipocyte differentiation. PloS one. 2008; 3:e2658. [PubMed: 18628823]
35. Soderberg O, et al. Characterizing proteins and their interactions in cells and tissues using the in situ proximity ligation assay. Methods. 2008; 45:227–232. [PubMed: 18620061]
36. Soderberg O, et al. Direct observation of individual endogenous protein complexes in situ by proximity ligation. Nature methods. 2006; 3:995–1000. [PubMed: 17072308]
37. Li Y, Krogh KA, Thayer SA. Epileptic stimulus increases Homer 1a expression to modulate endocannabinoid signaling in cultured hippocampal neurons. Neuropharmacology. 2012; 63:1140–1149. [PubMed: 22814532]
38. Nakamura T, et al. Inositol 1,4,5-trisphosphate (IP3)-mediated Ca2+ release evoked by metabotropic agonists and backpropagating action potentials in hippocampal CA1 pyramidal

neurons. The Journal of neuroscience : the official journal of the Society for Neuroscience. 2000; 20:8365–8376. [PubMed: 11069943]

39. Amundson J, Clapham D. Calcium waves. Current opinion in neurobiology. 1993; 3:375–382. [PubMed: 8396478]
40. Boehning D, Joseph SK. Direct association of ligand-binding and pore domains in homo- and heterotetrameric inositol 1,4,5-trisphosphate receptors. The EMBO journal. 2000; 19:5450–5459. [PubMed: 11032812]
41. Hetz C, et al. Proapoptotic BAX and BAK modulate the unfolded protein response by a direct interaction with IRE1alpha. Science. 2006; 312:572–576. [PubMed: 16645094]
42. Chen Y, Cantrell AR, Messing RO, Scheuer T, Catterall WA. Specific modulation of Na+ channels in hippocampal neurons by protein kinase C epsilon. The Journal of neuroscience : the official journal of the Society for Neuroscience. 2005; 25:507–513. [PubMed: 15647496]
43. Barnett ME, Madgwick DK, Takemoto DJ. Protein kinase C as a stress sensor. Cellular signalling. 2007; 19:1820–1829. [PubMed: 17629453]
44. Bright R, Mochly-Rosen D. The role of protein kinase C in cerebral ischemic and reperfusion injury. Stroke; a journal of cerebral circulation. 2005; 36:2781–2790.
45. Nagai K, Chiba A, Nishino T, Kubota T, Kawagishi H. Dilinoleoyl-phosphatidylethanolamine from Hericium erinaceum protects against ER stress-dependent Neuro2a cell death via protein kinase C pathway. The Journal of nutritional biochemistry. 2006; 17:525–530. [PubMed: 16426828]
46. Taylor CW, da Fonseca PCA, Morris EP. IP3 receptors: the search for structure. Trends in Biochemical Sciences. 2004; 29:210–219. [PubMed: 15082315]
47. Schmidt S, Ehrlich BE. Unloading Intracellular Calcium Stores Reveals Regionally Specific Functions. Neuron. 2010; 68:806–808. [PubMed: 21144994]
48. Chen X, et al. Endoplasmic reticulum Ca^{2+} dysregulation and endoplasmic reticulum stress following in vitro neuronal ischemia: role of Na+-K+-Cl-cotransporter. J Neurochem. 2008; 106:1563–1576. [PubMed: 18507737]
49. Yates D. Neurodegenerative disease: The stress of misfolding. Nat Rev Neurosci. 2012; 13:290–291. [PubMed: 22473482]
50. Gough NR. Neuronal ER Stress. Sci. Signal. 2010; 3:ec378-.
51. Green DR, Wang R. Calcium and Energy: Making the Cake and Eating It too? Cell. 2010; 142:200–202. [PubMed: 20655464]
52. Higo T, et al. Mechanism of ER stress-induced brain damage by IP(3) receptor. Neuron. 2010; 68:865–878. [PubMed: 21145001]
53. Luciani DS, et al. Roles of IP3R and RyR Ca2+ channels in endoplasmic reticulum stress and beta-cell death. Diabetes. 2009; 58:422–432. [PubMed: 19033399]
54. Taylor CW, Laude AJ. IP3 receptors and their regulation by calmodulin and cytosolic Ca2+. Cell calcium. 2002; 32:321–334. [PubMed: 12543092]
55. Chen R, et al. Bcl-2 functionally interacts with inositol 1,4,5-trisphosphate receptors to regulate calcium release from the ER in response to inositol 1,4,5-trisphosphate. The Journal of cell biology. 2004; 166:193–203. [PubMed: 15263017]
56. Boehning D, van Rossum DB, Patterson RL, Snyder SH. A peptide inhibitor of cytochrome c/inositol 1,4,5-trisphosphate receptor binding blocks intrinsic and extrinsic cell death pathways. Proc Natl Acad Sci U S A. 2005; 102:1466–1471. [PubMed: 15665074]
57. Higo T, et al. Subtype-specific and ER lumenal environment-dependent regulation of inositol 1,4,5-trisphosphate receptor type 1 by ERp44. Cell. 2005; 120:85–98. [PubMed: 15652484]
58. Hattori M, Higo T, Mikoshiba K. [Subtype-specific and ER lumenal environment-dependent regulation of IP3 receptor type 1 by ERp44]. Tanpakushitsu kakusan koso. Protein, nucleic acid, enzyme. 2005; 50:1292–1296.
59. Li G, et al. Role of ERO1-alpha-mediated stimulation of inositol 1,4,5-triphosphate receptor activity in endoplasmic reticulum stress-induced apoptosis. The Journal of cell biology. 2009; 186:783–792. [PubMed: 19752026]

60. Boehning D, van Rossum DB, Patterson RL, Snyder SH. A peptide inhibitor of cytochrome c/inositol 1,4,5-trisphosphate receptor binding blocks intrinsic and extrinsic cell death pathways. PNAS. 2005; 102:1466–1471. [PubMed: 15665074]

61. Fath T, Ke YD, Gunning P, Gotz J, Ittner LM. Primary support cultures of hippocampal and substantia nigra neurons. Nature protocols. 2009; 4:78–85. [PubMed: 19131959]

62. Li Y, Popko J, Krogh KA, Thayer SA. Epileptiform stimulus increases Homer 1a expression to modulate synapse number and activity in hippocampal cultures. J. Neurophysiol. 2013

63. Tiscornia G, Singer O, Verma IM. Production and purification of lentiviral vectors. Nature protocols. 2006; 1:241–245. [PubMed: 17406239]

64. Nicholson AM, Ferreira A. Increased membrane cholesterol might render mature hippocampal neurons more susceptible to beta-amyloid-induced calpain activation and tau toxicity. The Journal of neuroscience : the official journal of the Society for Neuroscience. 2009; 29:4640–4651. [PubMed: 19357288]

65. Keith, BJ.; Franklin, GP. The Mouse Brain in Stereotaxic Coordinates. Acdemic Press; 2008.

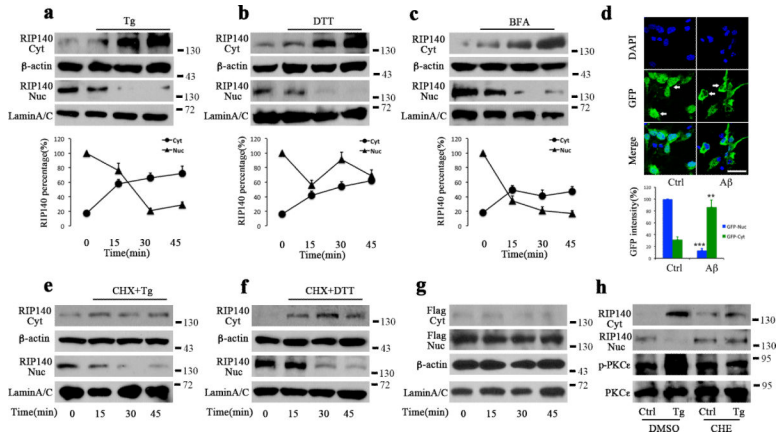

Figure 1. UPR induces RIP140 translocation to cytoplasm

a-c, Western blot analyses of changing levels of RIP140 in cytoplasmic (Cyt) and nuclear (Nuc) fractions of HT22 cells at the indicated time points following treatment with 1 μM thapsigargin(Tg), 2 μM dithiothreitol (DTT) and 5μM brefeldin A (BFA). The level of RIP140 relative to β-actin (cytoplasmic marker) or laminA/C (nuclear marker) is shown in the lower panel. **d,** Confocal microscopy shows representative images of green fluorescence in cultured hippocampal neurons infected with Lentivirus carrying GFP-RIP140. Nucleus is labeled with DAPI (blue) and arrows point to GFP-RIP140 retained in the nucleus in control, and those exported to the cytoplasm following treatment with 10 μM amyloid-beta (Aβ). Bar graph shows GFP intensity representing RIP140 level. Data from three independent experiments (37 cells from control group and 44 cells from Aβ–treated group) are presented as means ± SEM., **p=0.0087, ***p=0.00032 compared to control group as determined by Student's t-test. Scale bar, 20 μm. **e-f,** Western blot analyses of RIP140 level in Cyt and Nuc of HT22 cells exposed to 1μM Tg and 2μM DTT for the durations indicated in the presence of cycloheximide (CHX, 10 μM) to block translation. **g,** Western blot analyses of transfected Flag-RIP140 mutant (CN) in different fractions of HT22 cells treated with 1μM Tg. **h,** Western blot analyses of endogenous RIP140 level in Cyt and Nuc of HT22 cells treated with 1μM Tg following incubation with PKC inhibitor(CHE).

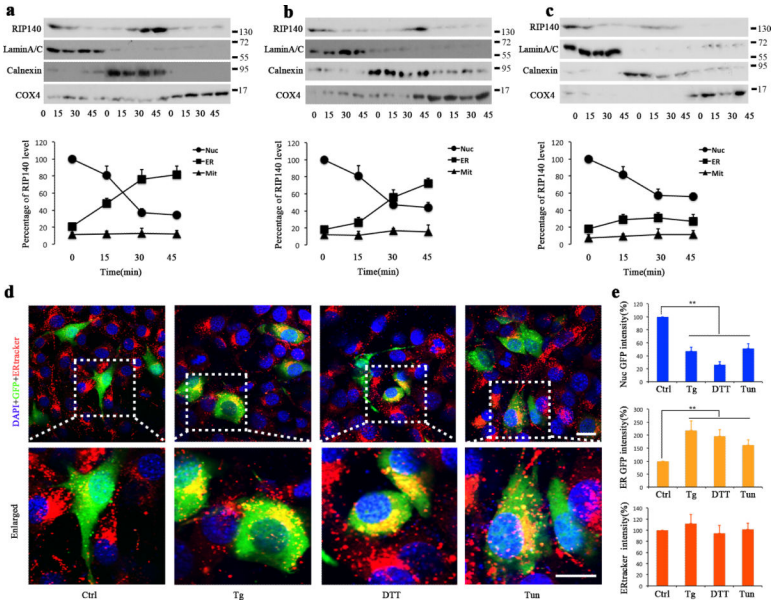

Figure 2. UPR induces translocation of RIP140 to the ER

a-c, Western blot analyses of RIP140 levels in nuclear (Nuc), endoplasmic reticulum (ER) and mitochondrial (Mit) fractions of HT22 cells at different time points following treatment with 1μM thapsigargin(Tg) (panel a), 2μM dithiothreitol (DTT) (panel b) or 500 μM tunicmycine(Tm) (panel c) treatment. The relative protein level was analyzed as a percentage of lamin A/C for nuclear, calnexin for ER and COX4 for Mit. The RIP140 level in Nuc of control group was calculated as 100%. **d**, Representative confocal microscopy images indicating RIP140 cytoplasmic translocation and localization to ER in HT22 cells after treatment with 1 μM Tg, 2 μM DTT and 50 μM Tm. Green fluorescence indicates infected cells with Lentivirus carrying GFP-RIP140. Red fluorescence shows ER tracker. Nuclei are labeled with DAPI (blue). Scale bars, 20 μm. **e**, Percentage of nuclear and cytoplasmic GFP fluorescence or red fluorescence intensity from three independent experiments (43 cells were included in each group), showing RIP140 and ER intensity, respectively, in treated cells compared to control cells. Results are presented as means ± SEM.,**p<0.01 compare to control group as determined by Student's t-test.

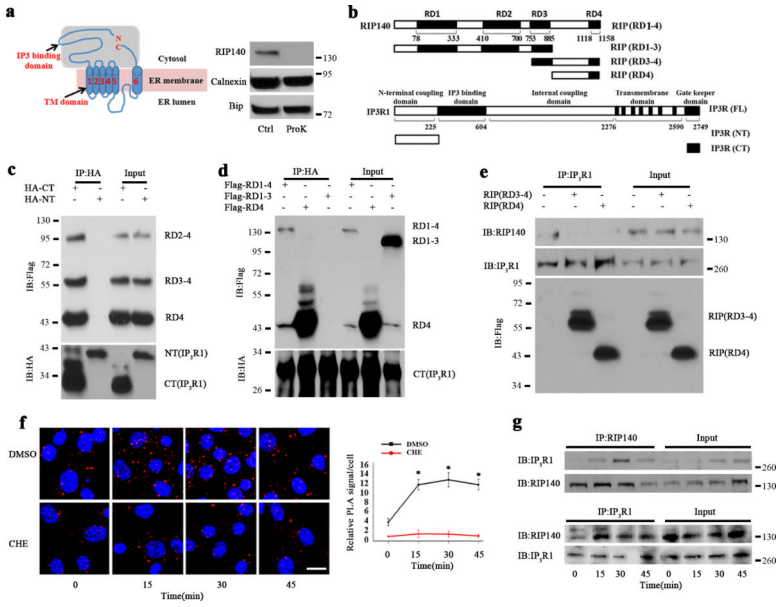

Figure 3. RIP140 interacts with IP_3R1

a, Western blot analysis of RIP140 in ER fraction treated with proteinase K (ProK) or without the enzyme (Ctrl). **b,** Constructs of RIP140 and IP_3R1. **c,** Reciprocal coimmunoprecipitation examining the interaction domain of IP_3R1 with RIP140. HT22 cells were transfected with HA-tagged N-terminal (NT) or C-terminal (CT) domain of IP_3R1 and flag-tagged RD2-4, RD3-4 and RD4 of RIP140. By coimmunopreciping with HA antibody, the flag-tagged domains of RIP140 can be detected only in the presence of CT. **d**, Reciprocal coimmunoprecipitation examining the interaction domain of RIP140 with IP_3R1. HT22 cells were transfected with HA-tagged C-terminal (CT) of IP_3R1 and flag-tagged RD1-4, RD4 and RD1-3 of RIP140. By coimmunopreciping with HA antibody, only the RD4-containing flag-tagged RIP140 can be detected. **e,** Competition of RD4, or RD4-containing RD(3-4), with the endogenous RIP140 for interacting with IP_3R1 in HT22. Cells were transfected with control vector, RD3-4 and RD4, the endogenous IP_3R1-interacting RIP140 was detected by RIP140 antibody that can only recognize N-terminal domain of RIP140. RD4 domain of RIP140 competes the binding of RIP140 to IP_3R1. **f,** Increased association of endogenous RIP140 with IP_3R1 monitored by *in situ* PLA assay in HT22 cells treated with thapsigargin for different durations. The red puncta show endogenous RIP140-IP_3R1 complexes. The graph shows statistical results presented as means ± SEM. from five independent experiments; *p<0.05 relative to the control group as determined by Student's *t*-test. Scale bar, 20 μm. **g,** Coimmunoprecipitation examining binding of RIP140 to IP_3R1 in HT22 following Tg treatment.

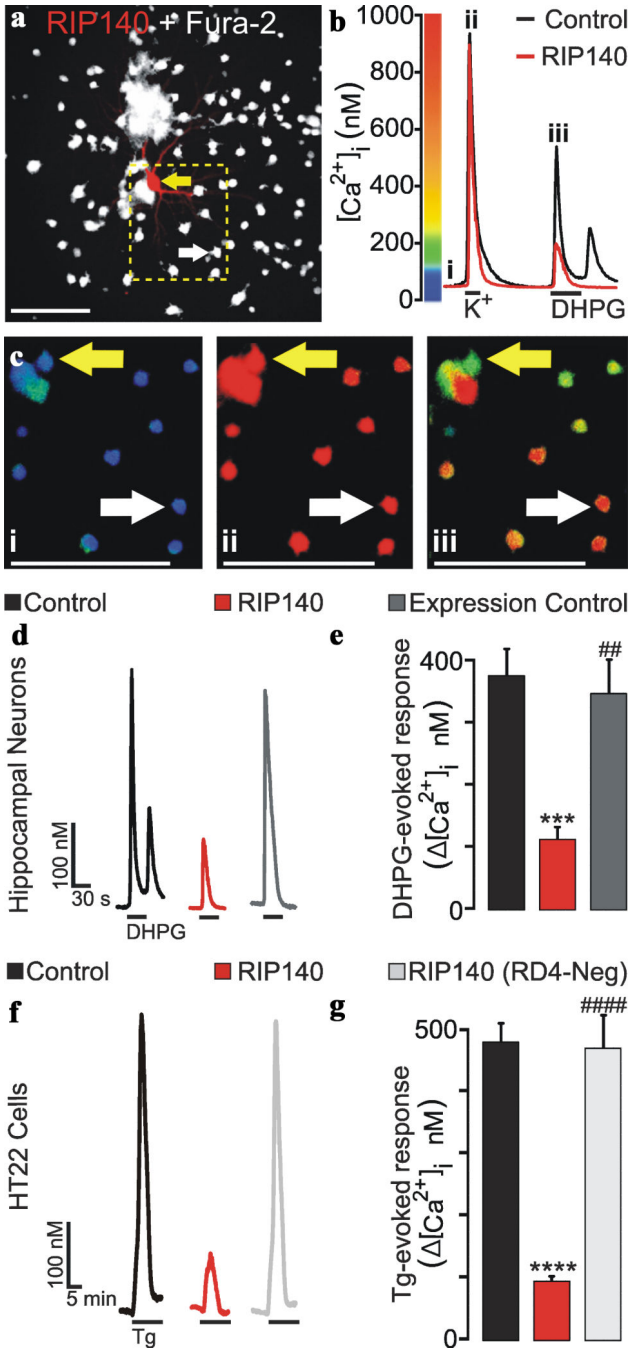

Fig. 4. RIP140 attenuates ER Ca^{2+} release in neurons

$[Ca^{2+}]_i$ was recorded using fura-2-based digital imaging (Methods). A, Representative image (n = 1 of 8) shows a neuron expressing RIP140 (⇦) and DsRed2 in a field of neurons loaded with fura-2 (⇨) (scale bar = 100 μm). Neuronal processes are not visible in the fura-2 image because it was focused to the center of the soma above the focal plane of the dendrites. B, representative trace shows $[Ca^{2+}]_i$ for the non-expressing (▬) and RIP140-expressing (▬) neurons identified by the arrows in A. Neurons were superfused with 50 mM K^+ and 30 μM DHPG at the times indicated by the horizontal bars

in B. C, pseudocolor images were scaled as shown in B. Images were collected at the times indicated by the lowercase numerals annotating the traces in B. D, representative traces show DHPG-evoked Ca^{2+} release from non-expressing neurons () and neurons expressing DsRed2 () or RIP140 (). E, Bar graph shows net $[Ca^{2+}]_i$ increase evoked by DHPG in non-expressing neurons () and neurons expressing DsRed2 () or RIP140 (). ***p<0.001 relative to non-expressing control; ##p<0.01 relative to RIP140 as determined by one-way ANOVA with 3 levels followed by Tukey's post test for multiple comparisons. E, representative traces show Ca^{2+} release evoked by 1 μM thapsigargin from non-expressing () HT22 cells and from HT22 cells expressing RIP140 () or RIP140 (RD4-neg) (). F, Bar graph shows net $[Ca^{2+}]_i$ increase evoked by Tg in non-expressing () HT22 cells and HT22 cells expressing RIP140 () or RIP140(RD4-neg) (). ****p<0.0001 relative to control; ####p<0.0001 relative to RIP140 as determined by one-way ANOVA with 3 levels followed by Tukey's post test for multiple comparisons.

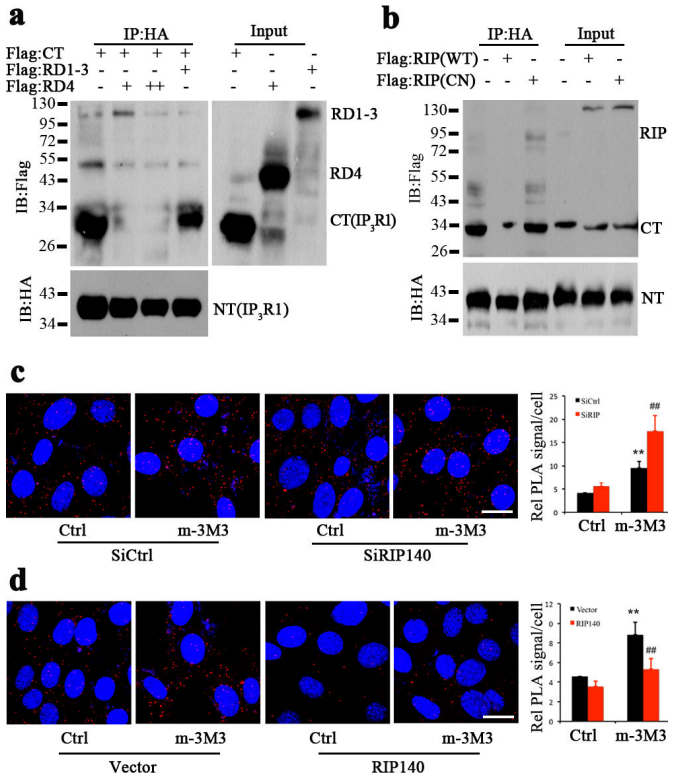

Figure 5. RIP140 interrupts "head-tail" interaction of IP_3R

a, *In vitro* competition assay using RD4 to compete out the binding of IP_3R1-NT to IP_3R1-CT. RIP140 RD1-3 was used as a negative control. Inputs correspond to 10% of flag-labeled protein as indicated. The binding of IP_3R-NT to IP3R-CT was significantly blocked by an increasing concentration (++) of RD4. **b,** Coimmunoprecipitation examining the effect of cytoplasmic RIP140 on IP_3R1 "head-tail" interaction. HT22 cells were transfected with HA-tagged C-terminus (CT) and flag-tagged N-terminus (NT) of IP_3R1 and flag-tagged wild-type RIP140 (WT) or mutant RIP140 (CN), which is localized in the nucleus. Only expressing WT RIP140, but not the mutant (CN), blocked IP_3R1 CT and NT interaction. **c-d,** The "head-tail" interaction of endogenous IP_3R1 was examined in HT22 cells. *In situ* PLA assay was used to monitor the interaction of endogenous IP_3R1's "head" (N-terminal suppressing domain) and "tail" (C-terminal gate-keeper domain) using antibodies specific to C- or N-terminus of IP_3R1. Red punctae show positive "head-tail" interaction of endogenous IP_3R1. "Head-tail" interaction was increased by applying the PLC activator m-3M3FBS (10 μM; m-3M3). The increased "head-tail" interaction was further enhanced following RIP140 knockdown(**c**), and was abolished upon RIP140 overexpression (**d**). The statistic results of "head-tail" interaction from three independent experiments (seven different fields from each experiment) are presented as means ± SEM., $^{**}p<0.01$ compare to control group; $^{\#\#}p<0.01$reletive to SiCtrl as determined by one-way ANOVA. Scale bars, 20 μm.

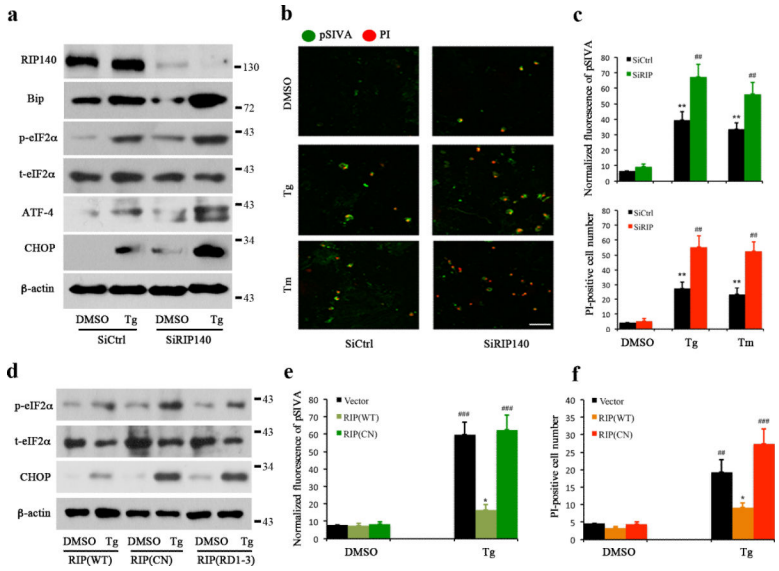

Figure 6. Interaction of RIP140 with IP_3R is required for its protective role against ER stress

a, Western blot analyses of ER-stress related protein levels in control (SiCtrl) or RIP140 knockdown (SiRIP140) HT22 cells treated with 1μM thapsigargin(Tg) for 3 h. **b,** Apoptotic cells were detected by pSIVA-PI positive staining in HT22 transfected with siRNA against RIP140 (SiRIP140) and treated with Tg or Tm for 3 h. Representative image of green fluorescence shows pSIVA staining and red fluorescence shows propidium iodide (PI). Scale bar, 40 μm. **c,** Quantified results of pSIVA intensity and PI-positive cell number. **d,** Western blot analyses of ER stress related proteins in response to Tg treatment in HT22 cells transfected with wild-type (WT) or mutated RIP140 (CN) and RIP1-3 of RIP140(RIP1-3). **e-f,** Quantified results of apoptotic cells detected by pSIVA (**e**) and PI (**f**)positive staining in HT22 cells expressing wild-type (WT) or mutated RIP140(CN) following treatment with Tg for 3 h. The pSIVA intensity and PI-positive cell number from seven different fields per group of three independent experiments are presented as means ± SEM., *p<0.05, **p<0.01 and ***p<0.001 relative to DMSO control group; ##p< 0.01, ###p< 0.001 reletive to treated SiCtrl and WT RIP140 transfected group as determined by one-way ANOVA, respectively.

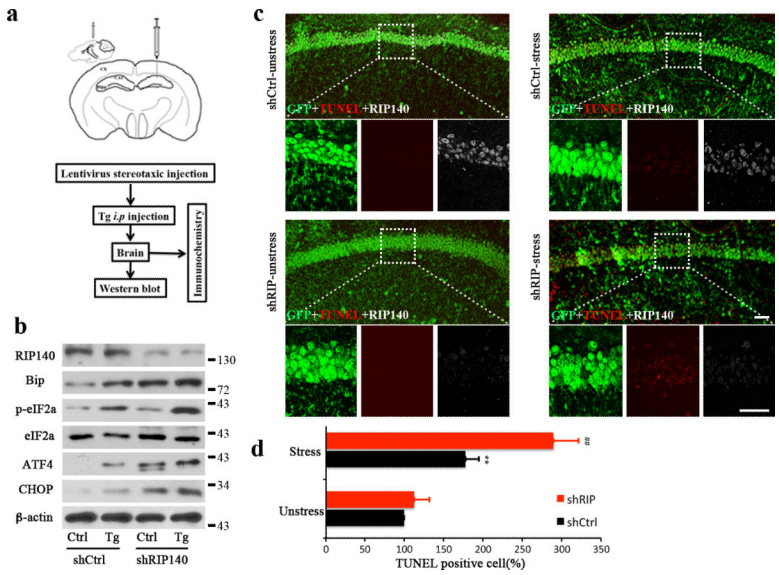

Figure 7. RIP140 protects cells from ER stress in mouse brain

a, Cartoon depicting the site of Lentiviral injection and the experimental procedure. **b,** Western blot analyses of RIP140 and ER stress related proteins Bip, p-eIF2a, ATF4 and CHOP in the virus-injected brain area 5 days after injection with lentivirus-ShRIP140 (Lenti-ShRIP140) or Lentivirus-control (Lenti-Ctrl). **c,** TUNEL staining (red puncta) of brain sections from the Lentivirus-infected areas 20 days after virus injection (2 days post stress induction). DAPI (blue) depicts nuclear staining and green signals show Lentivirus-infected cells. Scale bars, 20μm. **d,** Bar graph shows the percentage of TUNEL-positive cells versus total cell number from same field. The results from five different fields in each group are presented as means ± SEM., **p<0.01 compare to unstressed group; ##p < 0.01 relative to stressed Lenti-Ctrl group as determined by one-way ANOVA.